

Global dynamics of symmetric and asymmetric wakes

By **D. A. HAMMOND** AND **L. G. REDEKOPP**

Department of Aerospace Engineering, University of Southern California,
Los Angeles, CA 90089-1191, USA

(Received 30 May 1995 and in revised form 22 February 1996)

The two-dimensional wake–shear layer forming behind a rectangular-based forebody with independent ambient streams on either side of the forebody is examined by direct numerical simulation. Theoretical aspects of global modes and frequency selection criteria based on local and global stability arguments are tested by computing local stability properties using local, time-averaged velocity profiles obtained from the numerical simulations and making the parallel-flow approximation. The theoretical results based on the assumption of a slightly non-parallel, spatially developing flow are shown to provide a firm basis for the frequency selection of vortex shedding and for defining the conditions for its onset. Distributed suction or blowing applied at the base of the forebody is used as a means of wake flow modification. The critical suction velocity to suppress vortex shedding is calculated. It is shown that local directional control (i.e. vectoring) of the near-wake flow is possible, but only when all global modes are suppressed.

1. Introduction

The spatio-temporal dynamics of bluff-body wake flows has been clarified considerably in recent years. These advances have been realized through a variety of approaches including stability analyses, model studies, experiments and numerical simulations. One of the key concepts emerging from these different approaches, and one which has been particularly revealing, is that of a global mode which underlies the streamwise structure of the wake and its discrete frequency selection. The important concepts and discussions of the applicability of global modes to general flows, including wakes, are presented in the reviews by Huerre & Monkewitz (1990) and Monkewitz (1993). A principal motivation behind the present study is to test some of the detailed aspects of theoretical predictions concerning the destabilization and nonlinear structure of global modes by means of an interactive combination of numerical simulation and stability analysis. At the same time, the study is designed to explore some resulting ideas related to control and symmetry breaking in a spatially developing, quasi-parallel shear flow.

Bluff-body wakes are typical of a class of shear flows where local, time-averaged velocity profiles may undergo changes in the nature of the local instability at different spatial positions along the path of its streamwise development. In the near-wake region, where there is a large velocity deficit in local cross-stream profiles of mean velocity, the local flow is typically absolutely unstable: a band of instability waves exists with group velocities directed both upstream and downstream. In the far-wake region, where the velocity deficit is much smaller, the local flow is almost

always convectively unstable: the entire band of unstable wavenumbers propagates in the downstream direction. These properties have been clearly established by stability analyses of measured and model wake profiles (cf. Mattingly & Criminale 1972; Koch 1985; Triantafyllou, Triantafyllou & Chryssostomidis 1986; Triantafyllou, Kupfer & Bers 1987; Monkewitz 1988; and Hannemann & Oertel 1989).

The implications of such spatially varying stability properties for the global dynamics of a flow were subsequently examined theoretically and numerically using a model equation possessing generic, but spatially inhomogeneous, dispersive properties. In particular, Chomaz, Huerre & Redekopp (1988, 1991) demonstrated that flows of mixed stability type over their streamwise development can exhibit an internal resonance when a spatial region of absolute instability of 'sufficient size' is sandwiched within contiguous regions of convective instability. The resonance is self-excited and characterized by a sharp frequency selection. The onset of these spontaneous dynamics, which is analogous to that of wake flows as the Reynolds number exceeds the critical value for vortex shedding, occurs via a Hopf bifurcation. This latter fact was verified experimentally in wakes behind cylinders by Mathis, Provansal & Boyer (1984), Provansal, Mathis & Boyer (1987) and Sreenivasan, Strykowski & Olinger (1986). Some of the dynamical characteristics described above, together with some of the links to underlying stability properties, have also been observed in numerical simulations (cf. Triantafyllou *et al.* 1986; Zebib 1987; Hannemann & Oertel 1989; and Karniadakis & Triantafyllou 1989, 1992). More recently Schumm, Berger & Monkewitz (1994) have provided detailed experimental measurements in wakes behind several different bluff bodies further validating the applicability of a Stuart–Landau model for the onset of vortex shedding and the nature of the bifurcated state, together with its response to various control inputs.

The spatial structure of the post-bifurcation state (e.g. that of active vortex shedding) exhibits organized dynamics over streamwise length scales which are large in comparison to the streamwise scale of the pocket of absolute instability responsible for the appearance of the state. This dynamical state is termed a *global mode* since it is describable in terms of a *streamwise* eigenmode which is destabilized when a control parameter (e.g. the Reynolds number) exceeds a critical value. This critical value of the control parameter for global instability is typically considerably greater than the value of the control parameter for which local instability would be possible on a parallel flow basis. The global mode is damped in the pre-bifurcation state and it is spontaneously excited in the post-bifurcation state. It is worth noting that any observed global mode state is, in fact, a nonlinear entity since some self-limiting nonlinearity is required to achieve a realizable equilibrium state.

The important link between local instability properties and global dynamics in flows exhibiting internal, spontaneous resonances has been established theoretically via a slowly varying or WKBJ approach (cf. Chomaz *et al.* 1991; Monkewitz, Huerre & Chomaz 1993 and Le Dizès *et al.* 1996). This intimate, but powerful, link between local and global states is both appealing and useful for understanding the observed dynamics and for proposing scenarios, or the lack thereof, for flow manipulation. For example, the theory identifies a specific spatial position in the absolutely unstable region where an effective 'wave-maker' is positioned, providing a precise frequency selection criterion for the global mode at the bifurcation point. It also reveals the existence of some type of integral criterion for the initial destabilization of a global mode and provides some important insights pertaining to the forcing of these modes (cf. Chomaz, Huerre & Redekopp 1990). However, in many real flows the assumptions underlying the WKBJ approach are not approximated very closely. For

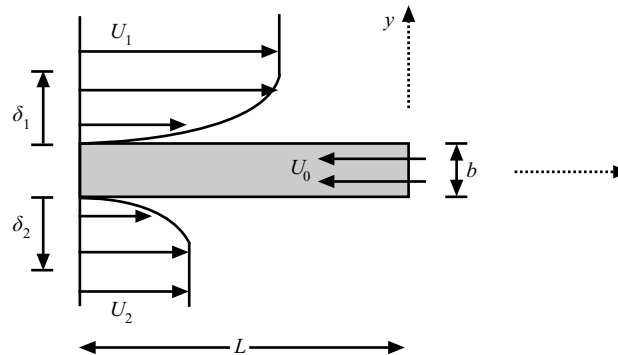


FIGURE 1. Flow configuration.

example, the spatially developing wake flow at conditions only slightly below the critical Reynolds number for onset of vortex shedding has local velocity profiles which are clearly unstable based on a parallel-flow approximation. Nevertheless, the pre-bifurcation state does not display any noise amplification of existing convective or absolute instabilities, evidently, because the spatial non-uniformity of the flow is so strong. Hence, there are two effects characterizing the wake at subcritical conditions: the strong spatial non-uniformity of the flow and the under-developed region of local absolute instability. Since vortex shedding is a global dynamical state and the marginally stable, subcritical state has locally unstable profiles, it seems clear that the streamwise non-uniformity of wake flows and their spatially varying stability properties are important features underlying the observed spatio-temporal dynamics of this class of free shear flows. Consequently there is a need to validate some of the theoretical predictions for global modes and to examine the robustness of these predictions in contexts where the underlying theoretical assumptions are violated. This forms the principal motivation for the present study. The results of the study reveal the utility of the theoretically established concepts and criteria.

2. Problem formulation

The general flow configuration studied here consists of two independent streams of incompressible fluid flowing parallel to each other on opposite sides of a (semi-infinite) body with a rectangular base. A wake forms downstream of the fixed separation points of the rectangular base. A sketch of the flow configuration is provided in figure 1. The ambient speeds of the two streams are specified independently so a persistent shear can be imposed across the developing wake. The base height b is used as the length scale and the average velocity U_∞ of the two streams is used as the reference velocity. With these scales, the relevant dimensionless parameters are the Reynolds number Re and the velocity ratio r defined as

$$Re = \frac{U_\infty b}{\nu}, \quad r = \frac{1}{2}(U_1 - U_2). \quad (2.1)$$

Note that U_1 and U_2 are dimensionless stream speeds scaled with the dimensional velocity U_∞ . The computational domain (nominally) extends from three units (i.e. a length equal to $3b$) upstream of the rectangular base of the forebody to 20 units

downstream. Convective outflow boundary conditions

$$\frac{\partial v}{\partial t} + u(x_e, y, t) \frac{\partial v}{\partial x} = 0, \quad (2.2)$$

where v is the velocity, are applied at the position x_e at the downstream end of the computational domain. The inlet flow is specified, on respective sides of the forebody, to consist of ambient streams with uniform streamwise velocities U_1 and U_2 contiguous with (nominally Blasius) boundary layers of thicknesses δ_1 and δ_2 adjacent to the parallel walls of the forebody. The lateral boundaries of the computational domain extend approximately 20 units on each side from the walls of the forebody. Along these boundaries the streamwise velocity is set equal to the respective ambient value and the perturbation pressure is supposed to vanish. The cross-stream velocity on these lateral boundaries is unspecified so that some weak inflow or outflow along these permeable boundaries is allowed. The no-slip conditions are applied along the walls of the forebody and the velocity vector is specified on the base so that arbitrary spatial distributions and angles of blowing or suction can be imposed as a means of wake flow modification. In what follows we suppose the dimensionless velocity U_0 is positive for base suction as shown in figure 1.

The direct numerical simulation of the two-dimensional, unsteady Navier–Stokes equations in primitive variables for an incompressible fluid was based on the QUICKEST (Quadratic Upwind Interpolation for Convective Kinetics with Estimated Streaming Terms) scheme proposed by Leonard (1979) and adapted by Davis & Moore (1982) and Davis, Moore & Purtell (1984). This finite-difference scheme was chosen because of its simplicity of implementation and it is easy to incorporate more complex geometric configurations like tandem wakes and two-dimensional jets. The production version of the code employed in the study presented here used a two-level grid. A uniform grid with $\Delta x = \Delta y = 0.1$ was used in the central streamwise strip extending from the edge of one boundary layer to the other boundary layer. In the regions external to this strip, the grid in the cross-stream direction was stretched by a factor of 8% per interval as one proceeds away from the wake. This is illustrated in figure 2.

The numerical simulation was validated by comparing the computed frequency of vortex shedding for symmetric flow (i.e. $r = 0$) with the numerical results reported by Hannemann & Oertel (1989). They studied the same flow, albeit with slightly different boundary layer in-flow. Using a Reynolds number of 200 and fixing the boundary layer thicknesses to be approximately equal to the values corresponding to their case, the shedding frequency (or Strouhal number when non-dimensionalized with the average velocity U_∞ and base height b) agreed to within 10% using the nominal grid defined above. Refinement of the grid by a factor of 2 resulted in only a 1% change in the shedding frequency. Another measure of the computational accuracy is to evaluate the degree to which mass is conserved. For simulations using the nominal grid, a global mass loss of 0.01% was found over a time period of 10 vortex-shedding periods. Tests were also made to evaluate the effect of the downstream boundary conditions, or the location where these conditions were applied. To this end, simulations were made for a symmetric wake ($r = 0$) in the absence of suction ($U_0 = 0$) at $Re = 320$ and with inlet boundary layer thicknesses of $\delta_1 = \delta_2 = 1.2$ where the downstream end of the computational domain was varied from 20 to 37 to 97 units from the base of the forebody. The shedding frequency was measured along with the amplitude (i.e. one-half the peak-to-peak value) of the velocity fluctuations (Δu_s , Δv_s) of the saturated shedding state at the fixed point ($x = 1$, $y = 1/2$) in the wake. The results are given in table 1. The

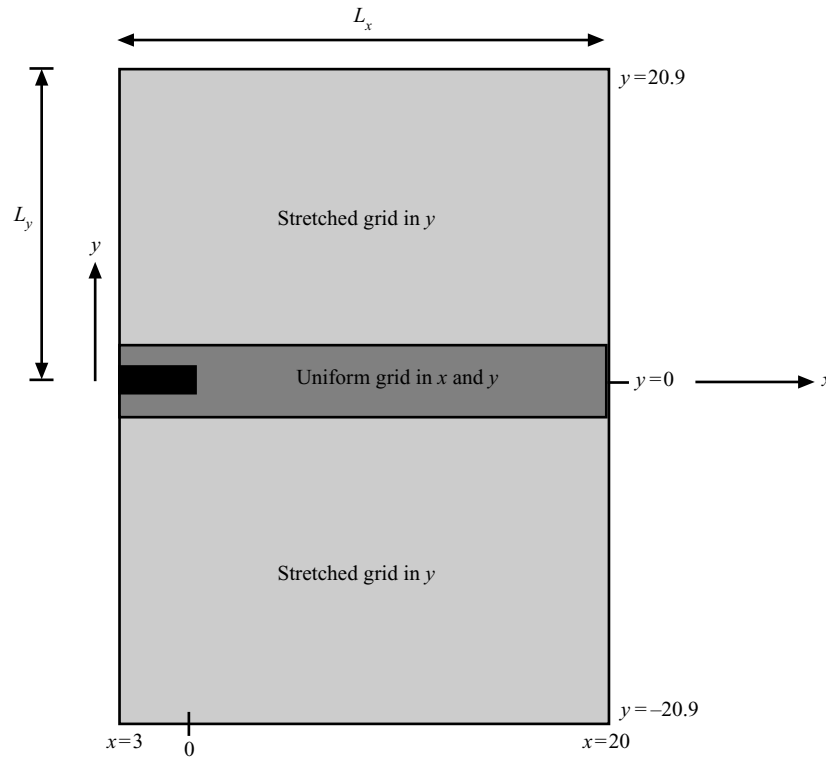


FIGURE 2. Computational domain with two-level grid.

	$-3 < x < 20$ $nx = 230$	$-3 < x < 37$ $nx = 400$	$-3 < x < 97$ $nx = 1000$
f	0.1065	0.1087	0.1086
Δu_s	0.0626	0.0626	0.0630
Δv_s	0.0725	0.0802	0.0807

TABLE 1. Results from a test of the position of the downstream boundary conditions.

shedding frequency increased by about 2% when the domain was extended from the nominal position of 20 units downstream. The amplitude of the streamwise velocity fluctuation was essentially constant while the amplitude of the transverse velocity fluctuation increased by about 10% in the extended domain. These results provided a basis for confidence in the code and the selected grid parameters. The shorter computational domain was used because the available computational resources were limited.

3. Global mode dynamics in a symmetric wake

Simulations for symmetric wake flows ($r = 0$) were performed to provide data sets which could be analysed for both their global dynamics and local stability properties. Simulations were performed for different Reynolds numbers in the absence of any base bleed or suction and with an inlet boundary layer thickness of $\delta = 1.2$ on each

side. The boundary layer thickness was chosen to be comparable to that used by Hannemann & Oertel (1989) and was not varied for the simulations described in this paper. If the boundary layer thickness is reduced much further, a refinement in the grid is required which in turn requires greater computational resources. The displacement thickness of the boundary layers for this choice of δ was computed to be $\delta^* = 0.396$ at one grid point upstream of separation and $Re = 160$. It varied only slightly (about 1%) over the Reynolds number range considered here. Ideally, the Reynolds number at separation should be based on the geometric base height plus the displacement thicknesses of the boundary layers, but we have chosen to always quote the Reynolds number as defined in (2.1) and as it would appear in the scaled equations of motion.

We present first results of a simulation performed at a slightly supercritical Reynolds number, $Re = 160$, which was used most comprehensively to make comparisons with theoretical predictions. Time series of the streamwise velocity and corresponding frequency spectra for the saturated vortex-shedding state obtained at different spatial positions in the wake are shown in figure 3. There is clearly a single fundamental frequency (i.e. Strouhal number) $f = 0.1$ that is uniform throughout the wake. The existence of a global frequency had been established in early studies by Kovasznay (1949) and Roshko (1954). However, some confusion arose after Tritton (1959) reported the existence of two frequencies in a cylinder wake when the Reynolds number was in a certain range. This was clarified by Williamson (1988, 1989) who showed that the double-frequency measurements were stimulated by end effects which could induce oblique vortex shedding across the entire span. Model studies by Albarède & Monkewitz (1992) and Park & Redekopp (1992) have shown that these three-dimensional effects can be understood in terms of spanwise-propagating phase modes. Williamson shows that, when end effects are eliminated, the wake remains two-dimensional with a single, global frequency for $Re < 180$ in cylinder wakes. This corresponds to a supercriticality parameter

$$\Delta = \frac{Re - Re_{cr}}{Re_{cr}} \quad (3.1)$$

of $\Delta \simeq 2.83$ assuming a value of $Re_{cr} = 47$. Computations by Karniadakis & Triantafyllou (1992) suggest that three-dimensional effects appear for $200 < Re < 210$, or $3.26 < \Delta < 3.47$, in cylinder wakes. In the present study we estimate $Re_{cr} \simeq 120$, which yields $\Delta = 0.33$ for the simulation at $Re = 160$ shown in figure 3. Furthermore, the highest Reynolds number considered is 520 corresponding to $\Delta = 3.33$.

Mean velocity profiles at various streamwise positions were computed for the saturated state in order to establish connections between local stability properties and global dynamics. The wavenumber k_{max} corresponding to the most amplified temporal instability mode at each streamwise station was computed using an Orr–Sommerfeld solver with $Re = 160$. This wavelength λ_{max} was compared with the length scale L for variation of the momentum thickness θ of the wake in order to obtain a measure of the non-parallel nature of the spatially developing flow in terms of the parameter

$$\epsilon = \frac{1}{k_{max}} \left(\frac{1}{\theta} \frac{d\theta}{dx} \right) = \frac{\lambda_{max}}{L}. \quad (3.2)$$

The variation of ϵ with the streamwise distance is shown in figure 4. It is clear that streamwise gradients in the developing mean flow are not necessarily small for, say, $x < 6$. Consequently, direct quantitative comparisons between the present results and asymptotic theories should not be expected to yield good correspondence.

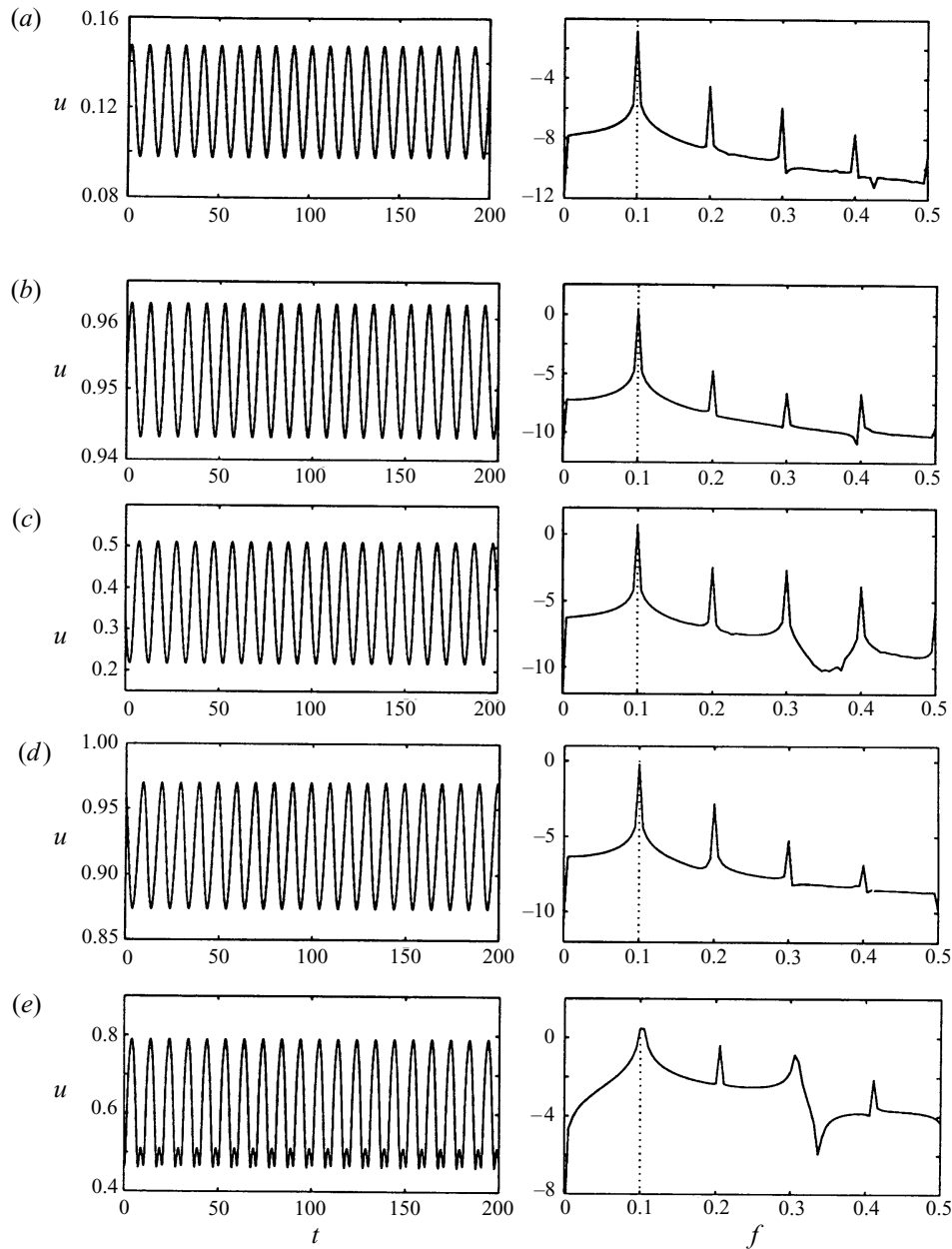


FIGURE 3. Time series and corresponding frequency spectra for the saturated wake at $Re = 160$ at different spatial locations: (a) $x = 1, y = 1.45$; (b) $x = 1, y = 1.45$; (c) $x = 5, y = 0.45$; (d) $x = 5, y = 1.45$; (e) $x = 10, y = 0.45$.

Frequency wavenumber pairs (ω_0, k_0) corresponding to the sinuous mode with vanishing group velocity (i.e. $\partial\omega/\partial k = 0$) were computed based on a locally parallel stability analysis of the mean velocity profiles at different streamwise positions. The results for $Re = 160$ are shown in figure 5. It is evident from the plot of the absolute growth rate $\omega_{0i}(x)$ that the wake is locally absolutely unstable for $0 < x < 3.15$. The global mode for this case, however, extends far beyond the point $x_{AU} = 3.15$.

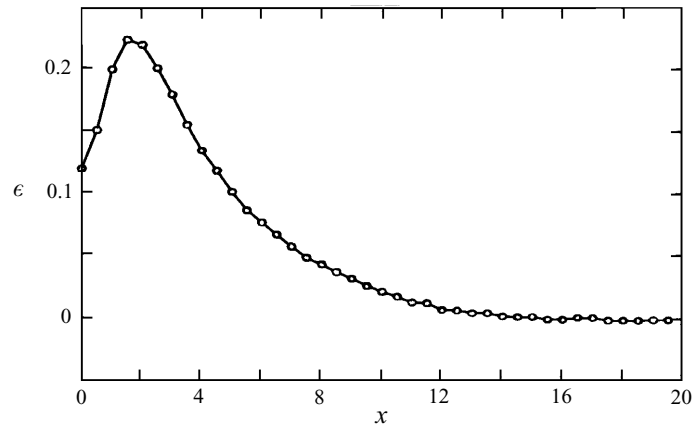


FIGURE 4. A measure of the non-parallel nature of the spatially developing wake at $Re = 160$.

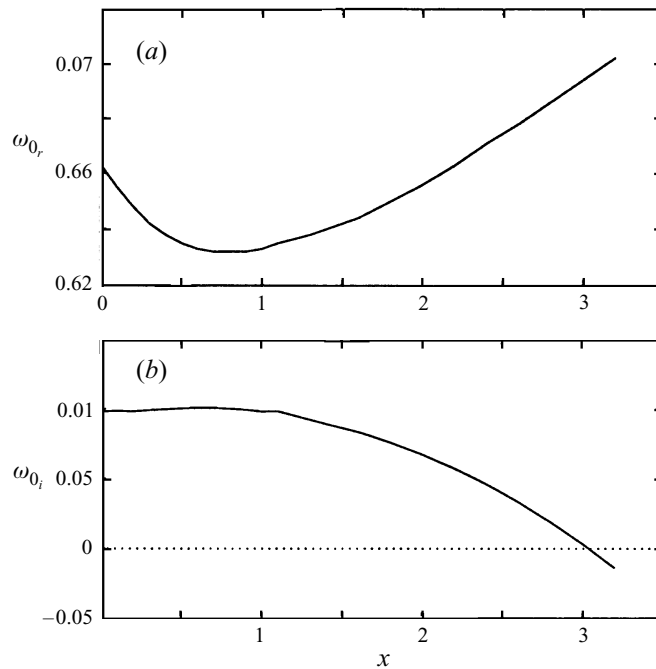
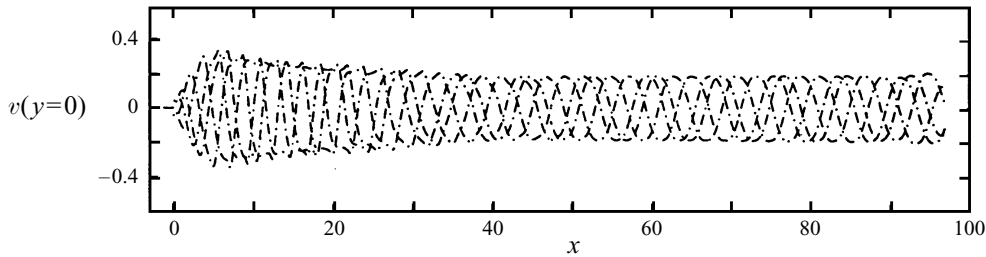


FIGURE 5. (a) The absolute frequency and (b) the absolute growth rate for the wake at $Re = 160$.

A representation of the global mode is shown in figure 6 where the transverse velocity along the wake centreline is plotted for four equally spaced phases of the vortex shedding cycle in the saturated state. For the purpose of computing the global mode in the present problem, the computational domain was extended to 100 base heights downstream of the forebody. However, as seen from figure 6, the global mode extends beyond the computational domain and encompasses a streamwise scale which is more than 30 times the length of the absolutely unstable pocket. By way of comparison, Kovasznay (1949) and Eisenlohr & Eckelmann (1988) suggest that the Kármán vortex street behind a cylinder extends (roughly) to 30 diameters downstream for Reynolds number not too far above the critical value. We point

FIGURE 6. The global mode structure in the wake at $Re = 320$.

out, parenthetically, that the results of figure 6 provide an excellent validation of the outflow boundary conditions. They are found to have no distinguishable effect on the structure of the global mode. In fact, the results in table 1 reveal that the shedding frequency varied by less than 2% when the computational domain size was increased from 20 to nearly 100 base heights behind the body.

Criteria for the existence of global mode dynamics in a spatially developing flow, and a prediction for the selection of the frequency of the mode, were advanced by Chomaz *et al.* (1991). They showed that a finite interval Δx_{AU} of local absolute instability was a necessary condition for the existence of a global mode, and that the frequency selected by that mode was equal to the real part of the absolute frequency ω_0 evaluated at the streamwise position x_s defined by

$$\left. \frac{\partial \omega_0}{\partial x} \right|_{x=x_s} = 0. \quad (3.3)$$

Close examination of figure 5 reveals that extrema of the curves $\omega_{0r}(x)$ and $\omega_{0i}(x)$ occur at different streamwise positions. This is clear evidence that the saddle point x_s does not lie on the real axis. However, since derivatives of $\omega_0(x)$ are only known along the real x -axis, the location of the saddle point x_s of $\omega_0(x)$ was found through use of the Cauchy–Riemann equations and analytic continuation to complex values of $x = x_r + ix_i$. This yields the expressions

$$\left. \begin{aligned} \omega_{0r}(x_s) &= \omega_{0r}(x_r, x_i = 0) - \left. \frac{\partial \omega_{0i}}{\partial x_r} \right|_{x_i=0} x_i + O(x_i^2), \\ \omega_{0i}(x_s) &= \omega_{0i}(x_r, x_i = 0) + \left. \frac{\partial \omega_{0r}}{\partial x_r} \right|_{x_i=0} x_i + O(x_i^2). \end{aligned} \right\} \quad (3.4)$$

Pairs of (x_r, x_i) are sought such that (3.3) is satisfied. The position of the saddle point for the symmetric wake at $Re = 160$ is $(x_{sr} = 0.79, x_{si} = 0.078)$. Straightforward application of the saddle-point criterion for the frequency selection of the global mode as computed based on local stability calculations yields the frequency $f_{sp} = (2\pi)^{-1} \omega_{0r}(x_s) = 0.1006$. This is compared with an observed frequency in the numerical simulation (obtained from spectra shown in figure 3) of $f = 0.1000$.

The correspondence is quite surprising since the saddle-point criterion is an asymptotic result and this comparison has ignored any corrections to the global mode frequency from higher-order effects such as mean flow non-uniformity, etc. Also, the analysed state is somewhat removed from the bifurcation point ($\Delta = 0.33$) and nonlinear corrections could be significant. The close correspondence between the predicted frequency based on the saddle-point criterion and the computed value may be fortuitous in that the various corrections could be self-cancelling. In order to

quantify some of these effects, and to provide the most comprehensive comparison with the asymptotic theory, the first linear correction based on the analysis presented by Monkewitz *et al.* (1993) was computed as well. The definition of the different correction terms and how they are computed based on the numerically obtained mean-flow profiles is described in the Appendix.

Although the work by Chomaz *et al.* (1991), and more recently by Le Dizès *et al.* (1996), has shown that a necessary condition for the existence of an observable (i.e. linearly unstable) global mode is that a finite interval of locally absolutely unstable flow be present, no definitive global criterion for predicting the condition or control parameter setting for onset is available. Using several model studies of the linear Ginzburg–Landau equation, Chomaz *et al.* (1990) conjectured that destabilization of the gravest global mode and the onset of global dynamics might be described by the condition

$$I_{AU} = \int_{\Delta x_{AU}} [\omega_0(x)]^{1/2} dx > M, \quad (3.5)$$

where M is some order-one constant. For the symmetric wake at $Re = 160$ shown in figures 5 and 6, $I_{AU} = 0.795$. We emphasize that this criterion does not have a rigorous asymptotic basis, but we expect that it might have some utility, especially when the absolute frequency $\omega_0(x)$ has an isolated saddle point which is not too far from the real axis. What it does imply is that the length of the absolutely unstable pocket has a more significant role than the magnitude of the absolute growth rate. As such, flow modification influencing Δx_{AU} can be expected to be especially influential in altering the conditions for onset. Of course, modifying the level of the absolute growth rate will likely accompany any modification affecting the streamwise extent of local absolute instability. Further results related to this point will be presented later.

The critical Reynolds number $Re_{cr} \simeq 120$ for the onset of vortex shedding was estimated by exploiting the established fact (see Provansal *et al.* 1987 and Sreenivasan *et al.* 1986) that vortex shedding appears spontaneously via a Hopf bifurcation. Consequently, the square of the saturation fluctuation amplitude at any point should scale linearly with the distance from the bifurcation ($Re - Re_{cr}$) (see (3.7) below). Results of this type are shown in figure 7 for the transverse and streamwise velocity components at a fixed point $(x, y) = (1.0, 0.5)$ in the wake. No attempt was made to choose the time series at the position where the global mode was a maximum in each realization (see figure 6). There may be some (possibly small) variation in the amplitude of the global mode at a fixed point that derives solely from shape changes as a function of Δ . Nevertheless, the bifurcation was supercritical and there appears to be a substantial range of parameter values where the described scaling behaviour applies. Schumm *et al.* (1994) arrived at the same conclusion based on their analysis of data from several different wake flows.

The computed dynamics can be described in terms of the Landau model for the complex amplitude of the global mode at a fixed spatial position. For this purpose, the model is written as

$$\frac{dA}{dt} = \sigma A - \beta |A|^2 A \quad (3.6)$$

where σ is the (complex) growth rate and β is the (complex) Landau constant. With the constraints that $\sigma_r(Re_{cr}) = 0$ and that σ_r varies linearly with distance from the

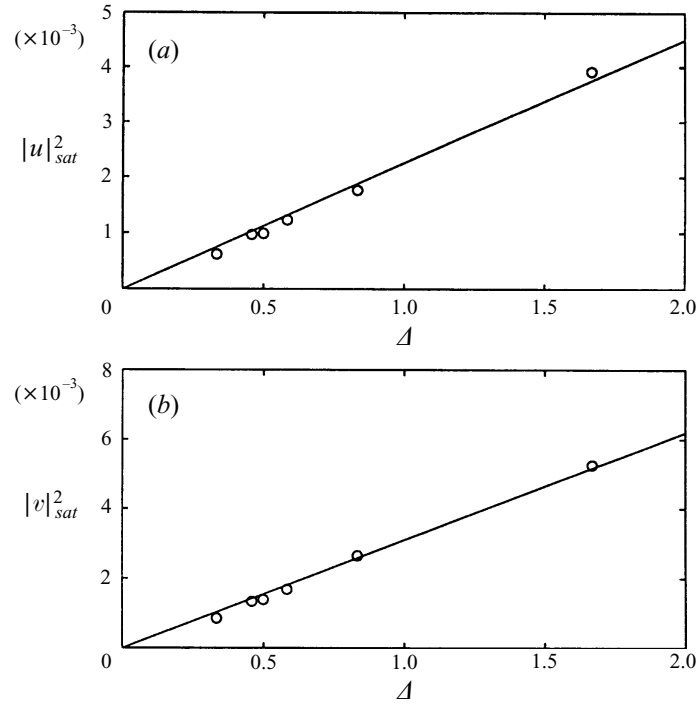


FIGURE 7. The square of the saturation amplitude of (a) the streamwise velocity component and (b) the cross-stream velocity component in the wake and its dependence on the supercriticality of the flow.

bifurcation point, one can write

$$|A|_{sat}^2 = \frac{\sigma_r}{\beta_r} = \frac{1}{\beta_r} \left. \frac{d\sigma_r}{dRe} \right|_{Re_{cr}} (Re - Re_{cr}), \quad (3.7)$$

$$\frac{1}{|A|} \frac{d|A|}{dt} = \sigma_r \left(1 - \frac{|A|^2}{|A|_{sat}^2} \right) \quad (3.8)$$

and

$$\frac{d\theta}{dt} = \sigma_i - \sigma_r \frac{\beta_i}{\beta_r} \frac{|A|^2}{|A|_{sat}^2}, \quad (3.9)$$

where θ is the phase of the complex amplitude A . The temporal growth rate of the global mode was determined following the approach utilized by Schumm *et al.* (1994). Using the modulus of the streamwise velocity at a fixed spatial position ($x = 1.0$, $y = 0.5$ in this case) for a slightly supercritical Reynolds number $Re = 140$ ($\Delta = 0.167$), we obtain $(d\sigma_r/dRe)|_{Re_{cr}} = 0.0078 \pm 0.0002$ (cf. figure 8b). In the same way, $\sigma_i = 2\pi f = 2\pi(0.0967 \pm 0.0002)$ (cf. figure 8c). The difference between the linear and the saturated values of the frequency yielded the normalized Landau constant $\beta_i/\beta_r = -1.37 \pm 0.30$. These calculations were repeated at various spatial locations in the wake to verify that the ‘constants’ were not spatially dependent. The corrections for the respective constants quoted above encompass the variations found from the time series at different spatial positions.

A number of researchers (e.g. Sreenivasan *et al.* 1986 and Williamson 1989) have shown that there is a linear increase in the Strouhal number with Reynolds number

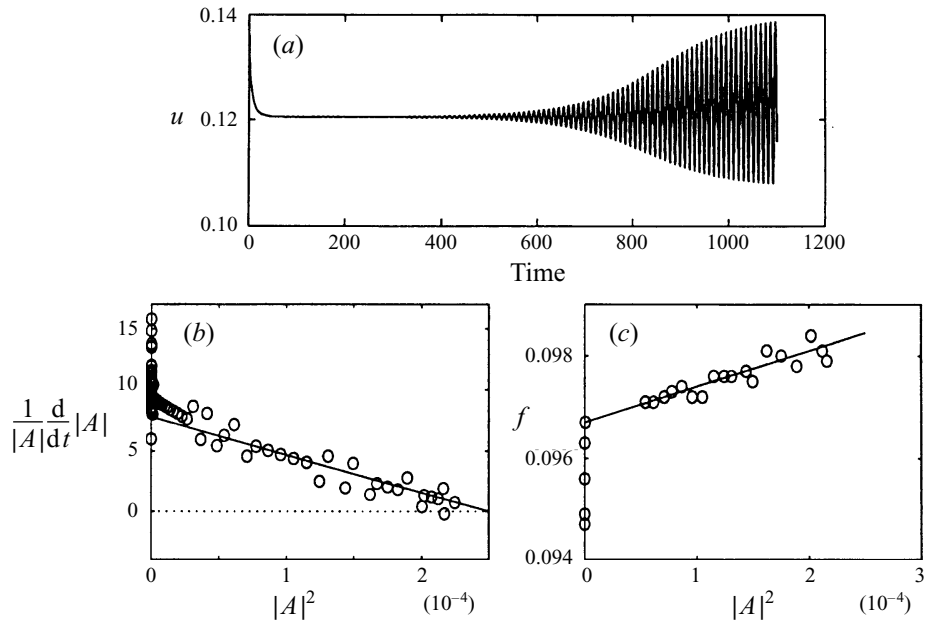


FIGURE 8. (a) The time series of the streamwise velocity component in the wake at $x = 1$ and $y = 0.5$ along with the corresponding temporal development of (b) the amplitude of the streamwise velocity component and (c) the vortex shedding frequency at $Re = 140$.

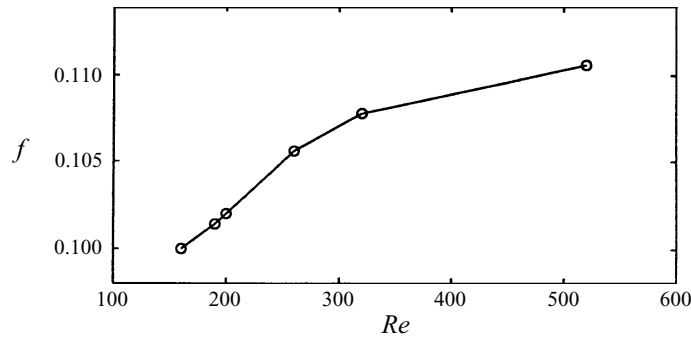


FIGURE 9. Vortex shedding frequency versus Reynolds number.

for Reynolds numbers slightly above critical. In their simulation of the symmetric wake behind a rectangular forebody similar to that studied here, Hannemann & Oertel (1989) reported a Strouhal number of 0.113 at $Re = 200$. We find a value of $f = 0.102$ at $Re = 200$, a value which is 11% smaller. However, direct comparisons should employ a Reynolds number which accounts for the displacement thicknesses of the boundary layers at separation. Since Hannemann & Oertel (1989) do not report computations of the displacement thicknesses at the trailing edge, the discrepancy in observed shedding frequency cannot be rationalized. On the other hand, Eisenlohr & Eckelmann (1988) report a universal Strouhal–Reynolds number curve for wakes behind bluff rectangular bodies which includes the displacement effect. Using a Reynolds number based on the base height plus displacement thicknesses, we obtain $f = 0.184$ compared to $f = 0.177$ (a difference of 4%) by Eisenlohr & Eckelmann (1988) at identical values of the adjusted Reynolds numbers. This provides further

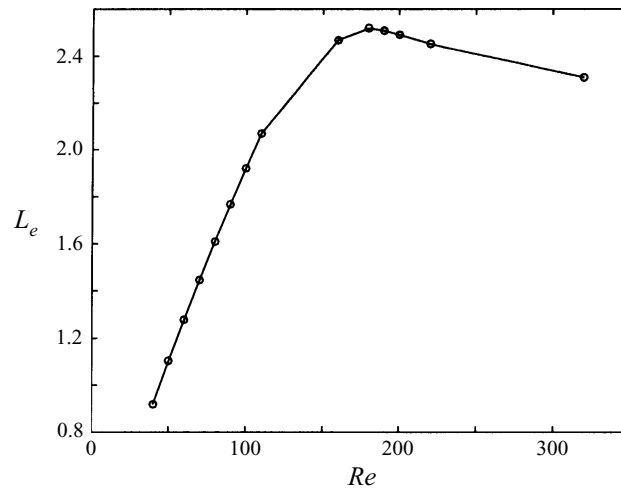


FIGURE 10. The length of the recirculation zone of the steady or time-averaged mean flow and its relation to the Reynolds number.

validation of our numerical results. The Strouhal–Reynolds number (i.e. f vs. Re) variation from our simulations of the symmetric wake is shown in figure 9. The Reynolds number used here excludes the displacement effect. Since the displacement thickness was (nearly) constant over the range of Reynolds numbers studied and the sum of the displacement thicknesses was 0.792 (scaled by the base height), the adjusted Reynolds number is readily obtained by multiplying by the factor 1.792.

Another measure of the symmetric wake is the streamwise distance L_e from the base of the forebody to the location of the near-wake saddle point in the streamline pattern. This is the length of the steady recirculating eddies at subcritical Reynolds numbers and the distance over which reversed flow is present in the time-average mean flow at supercritical Reynolds numbers. This length is shown in figure 10. Reference to figure 5 shows, at least for $Re = 160$, that $L_e < x_{AU}$.

4. Global mode dynamics in asymmetric wakes

One objective of this study was to investigate how the development of the wake is affected by a breaking in the symmetry of the mean flow. The measure of the symmetry of the mean flow is the velocity ratio r defined in (2.1). When r is non-zero, the flow will initially appear wake-like with a large velocity deficit. However, as the two layers of oppositely signed vorticity merge and the deficit relaxes, the flow will eventually transition from a wake flow to a shear layer flow. There is some question as to how this asymmetry will affect the structure of the global mode and how the vortex roll-up transitions from the familiar Kármán street to that of a shear layer where all vortices have the same sign. To this end, a number of simulations were performed for different velocity ratios. Throughout this study we assume that the high-speed stream is on the top ($y > 0$).

First, simulations were performed to establish the effect of mean flow asymmetry on the shedding frequency and the critical Reynolds number. Results of these simulations are shown in figures 11 and 12. The shedding frequency, at fixed Reynolds number, increases slightly with the velocity ratio. However, the critical Reynolds number decreases as the asymmetry of the ambient flow increases. The simulations shown

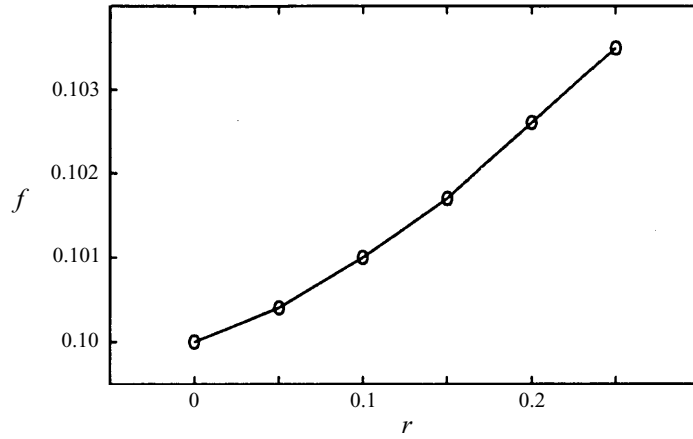


FIGURE 11. The vortex shedding frequency of the asymmetric wake at $Re = 160$.

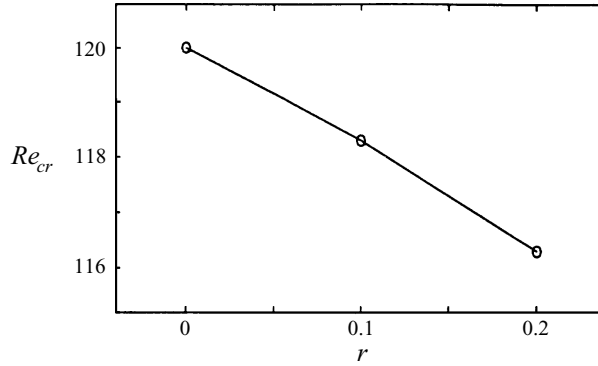


FIGURE 12. The critical Reynolds number of the asymmetric wake.

in figure 11 for $Re = 160$ were examined in more detail by taking local velocity profiles obtained from the time-averaged flow of the saturated state at each velocity ratio. The absolute frequency $\omega_0(x)$ was computed at different streamwise positions using the Orr–Sommerfeld solver together with the branch-point search algorithm. The distributions of $\omega_0(x)$, and the associated value $k_0(x)$, are presented in figure 13. Results are shown for the symmetric wake and two non-zero values of the velocity ratio. It is evident from figure 13(b) that the absolute growth rates are diminished by the effect of shear. Since these results are obtained for a fixed Reynolds number, and the critical Reynolds number decreases with increasing r , the effect of shear in decreasing the absolute growth rates would be even more pronounced if calculations were compared for fixed values of the supercriticality parameter Δ . Asterisks appearing on the curves in figures 13(a, b) indicate the position along the real x -axis of the saddle point x_s (cf. (3.3)). One also observes from figure 13(b) that the streamwise extent of the absolutely unstable region decreases with increasing r . As a result, evaluation of the integral quantity I in (3.5) will decrease with increasing asymmetry due both to a reduction in Δx_{AU} and in the magnitudes of $\omega_0(x)$. These effects are shown graphically in figure 14.

The frequency selection criterion discussed previously and defined by (3.3) was compared using the simulations corresponding to the results presented in figures 5

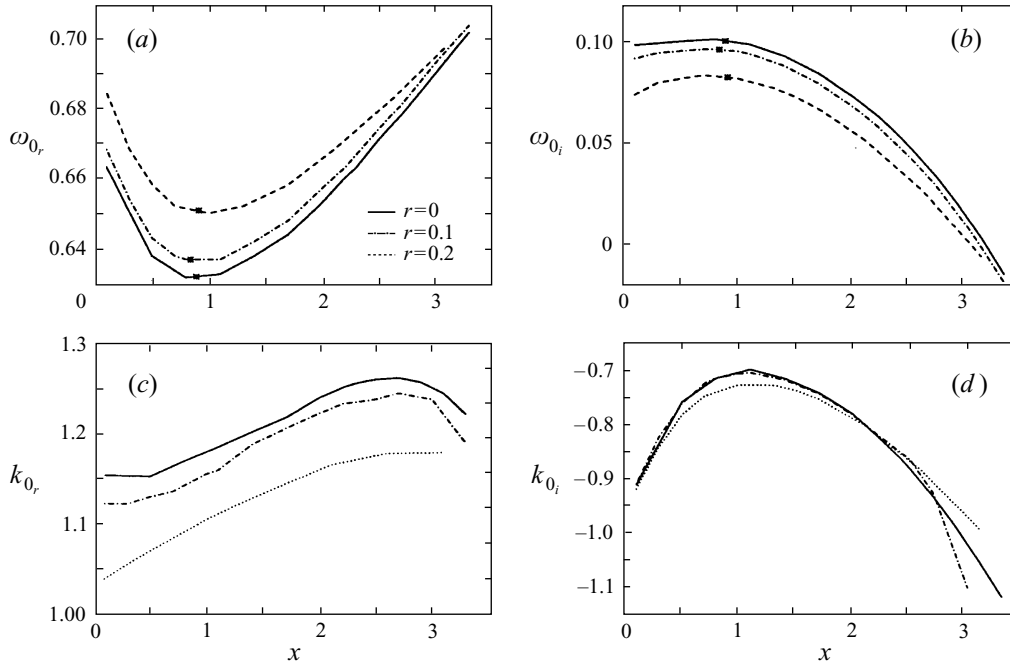


FIGURE 13. The streamwise development of (a,b) the absolute frequency and (c,d) the absolute wavenumber of the asymmetric wake at $Re = 160$.

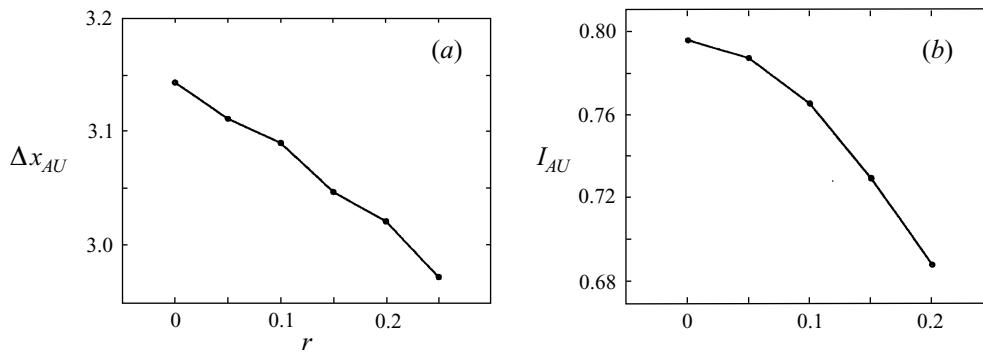


FIGURE 14. (a) The streamwise extent of the region of absolute instability and (b) the size of the absolute instability region as measured by the parameter I_{AU} for the asymmetric wake at $Re = 160$.

and 13. The leading-order asymptotic prediction of the frequency $f_{sp} = (2\pi)^{-1}\omega_{0,r}(x_{sr})$ was evaluated for several velocity ratios. The results are tabulated in table 2. The differences between the observed frequency and that determined by the saddle-point criterion are less than 2% in all cases. The correspondence is quite surprising since there are corrections arising from the non-parallelism of the flow, as defined in the Appendix, and the nonlinear nature of the global mode. It is important to point out that the calculation of f_{sp} already contains some nonlinear contributions, principally those arising from mean flow corrections. Mean flow velocity profiles obtained from a numerical simulation of the full unsteady equations of motion (i.e. vortex shedding active) at a supercritical Reynolds number were used in the local

r	x_{sr}	x_{si}	f	f_{sp}	f_k	f_p
0.00	0.79	0.078	0.1000	0.1006	0.1106	0.1007
0.05	0.74	0.069	0.1004	0.1008	0.1108	0.1007
0.10	0.74	0.066	0.1010	0.1014	0.1103	0.1014
0.15	0.76	0.081	0.1017	0.1023	0.1109	0.1023
0.20	0.81	0.132	0.1026	0.1035	0.1106	0.1038
0.25	0.82	0.128	0.1035	0.1050	0.1108	0.1049

TABLE 2. Saddle-point data and comparison of frequency selection criteria for asymmetric wakes at $Re = 160$.

instability calculations underlying the prediction of f_{sp} reported here. A better test of the theoretical underpinnings would employ velocity profiles from a completely steady simulation (i.e. vortex shedding absent) at the prescribed supercritical Reynolds number. The nonlinear correction from the mean flow correction is expected to be rather weak with a supercriticality parameter $\Delta = 0.33$, but no quantitative test of this exists. One could also consider smaller values of Δ , but transients decay much more slowly as Δ is decreased toward zero.

Alternative *ad hoc* proposals for the frequency selection for a global mode in a spatially developing flow have been advanced by Koch (1985) and by Pierrehumbert (1984). Koch proposed a frequency selection based on the downstream transition point where the flow instability type changes from absolute to convective. This frequency is denoted f_k in table 2. Pierrehumbert proposed that the frequency selected by the global mode corresponds to the real value of the absolute frequency ω_{0r} at the point where the absolute growth rate ω_{0i} achieves a maximum. This frequency is denoted by f_p in table 2. The value of f_p will be equal to f_{sp} when the saddle point lies on the real x -axis. However, this implies that the length of the absolutely unstable region is marginally equal to zero. It is evident from figures 13(a,b) that f_p differs, in the present simulations, only slightly from that given by the saddle-point selection criterion. This is because the saddle point is found to lie relatively close to the real x -axis. In any case, the saddle-point selection criterion is found to provide the best estimate. Of course, there is a rigorous basis for the latter criterion.

It is evident from the foregoing results that the strength or vigour of the global mode will decline as the shear or mean flow asymmetry is increased. This rather qualitative remark is made slightly more quantitative by exhibiting in figure 15 the entire global mode for different velocity ratios at a fixed Reynolds number $Re = 320$. In this figure the transverse velocity along the centreline ($y = 0$) of the wake is shown at four different phases of the saturated global mode. We have not attempted a comprehensive scaling of the global mode structure along the lines performed by Goujon-Durand, Jenffer & Wesfreid (1994) for the wake of a circular cylinder. The asymmetry in the present case of the mode about the $y = 0$ axis for $r \neq 0$ is evidence of the asymmetric transverse eigenfunction structure. The eigenfunction amplitude is greater for $y > 0$, where the vorticity is larger and the velocity difference across the shear layer is greater, than it is for $y < 0$. One observes also a clear diminution in the length of the global mode as the shear is increased. Now the streamwise structure of the global mode establishes the amplitude distribution of the synchronized dynamics; it does not reflect the strength of the local vorticity concentrations. The latter is described by the transverse eigenfunction and the magnitude of the phase velocity c relative to the local mean velocity profile $U(y)$ at any location x . For example,

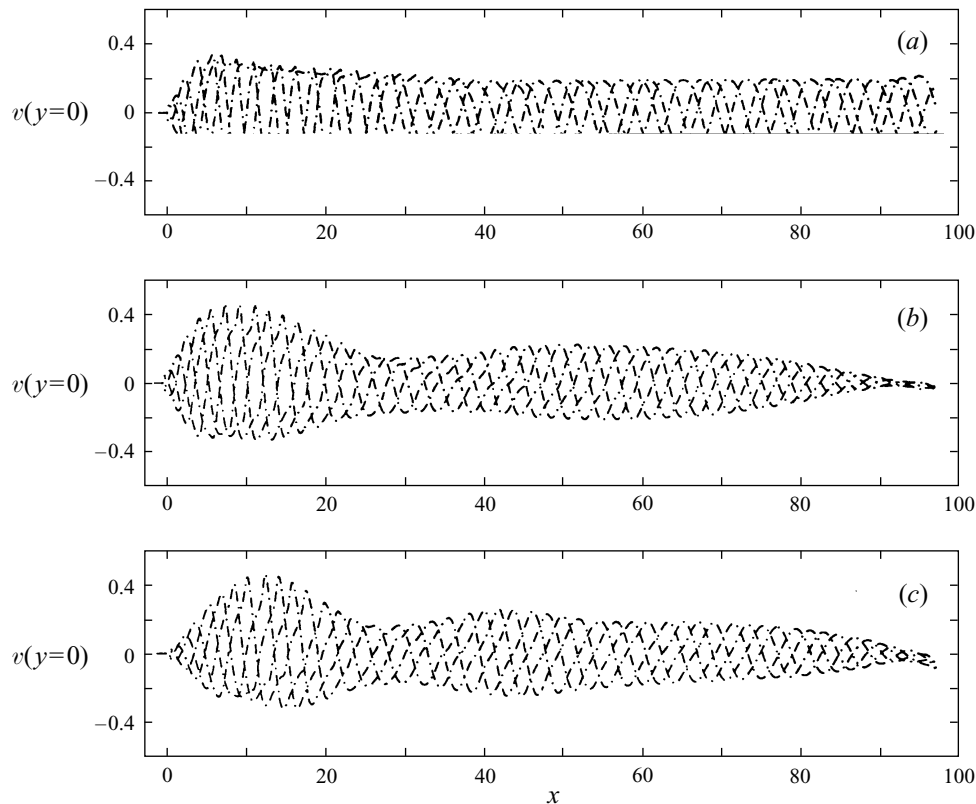


FIGURE 15. The global mode structure at $Re = 320$ for (a) $r = 0$, (b) $r = 0.1$, (c) $r = 0.2$.

if two critical levels exist (i.e. two zeros in the function $U(y) - c$), then there will exist two levels where concentrations of vorticity of opposite sign will form as in the familiar vortex street. However, when the velocity deficit in the wake diminishes with a fixed velocity ratio, only one critical level exists and vorticity concentrations of only one sign, that associated with the shear across the wake, will form. The wake will then transition to a shear layer. It is entirely possible for this transition to occur at some streamwise location within the active domain of the global mode. The vorticity structures in wakes having different velocity ratios are shown in figure 16. The transition from the wake mode to the shear layer mode is especially evident in figure 16(c) where a simulation with $r = 0.2$ is shown. The vorticity contours in figure 16 are drawn using the same level values in each of the panels.

Wallace & Redekopp (1992) discussed the transition from a wake mode to a shear layer mode in the context of linear stability theory using wake–shear layer profiles having the velocity deficit and the velocity ratio as parameters. They suggested that a possible measure of where this change in the vorticity distribution from a wake form to a shear layer form occurs might be the streamwise position where the sinuous mode of instability with the maximum spatial growth rate transitions from two critical levels to one critical level. Of course, there is no apparent relation between the most amplified wave according to local linear spatial stability theory and the characteristics of the saturated, supercritical global mode. Nevertheless, this is a well-defined criterion and one that is, at least, quite reasonable for convectively

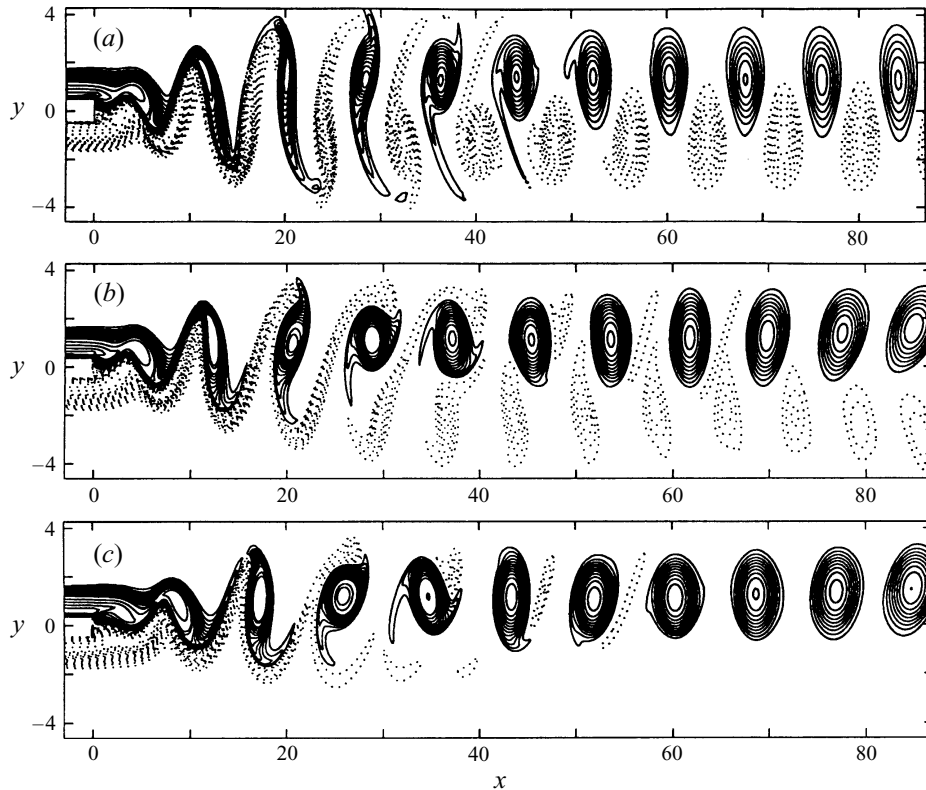


FIGURE 16. Vorticity contours (—, negative vorticity; ·····, positive vorticity) at $Re = 320$ for (a) $r = 0$, (b) $r = 0.1$, (c) $r = 0.2$.

	$Re = 160$	$Re = 320$
$r = 0.1$	15.9	12.8
$r = 0.2$	9.4	6.3

TABLE 3. Transition-point data for x_t based on spatial stability theory.

unstable flows. Computations based on local mean velocity profiles from the present numerical simulations yield the transition points x_t listed in table 3.

5. The effect of suction

A number of different techniques have been proposed for modifying or suppressing the vortex shedding from bluff bodies with the important practical goal of reducing the pressure drag on the body. Monkewitz (1989, 1993) has categorized these approaches to wake control in terms of open-loop and closed-loop control. One of the earliest approaches was that proposed by Roshko (1954) where a thin splitter plate aligned with the free-stream flow was strategically placed along the centreline of the near wake. His experimental results proved quite encouraging. Recently, this approach was explored further through numerical simulations by Grinstein, Boris & Griffin (1991). From the point of view of global modes, one might anticipate that this approach to

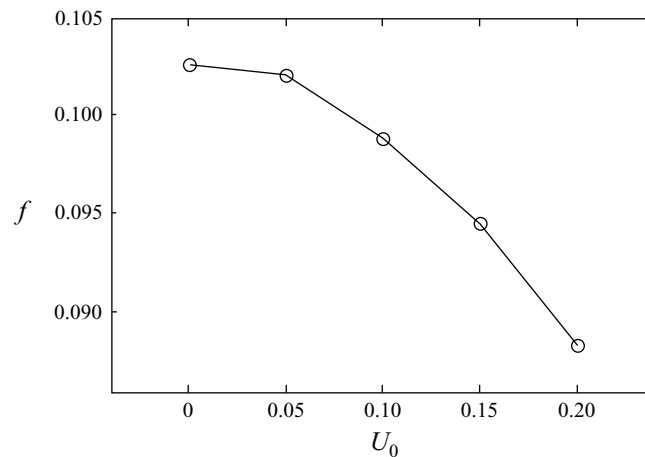


FIGURE 17. The dependence of the vortex shedding frequency of the asymmetric wake ($r = 0.2$) at $Re = 160$ on the trailing-edge suction velocity.

wake modification will be most efficient if the control plate is centred around the location of the saddle point of the absolute frequency (cf. (3.3)). However, we are not aware of any studies to date which have explored this connection with wake control. The control of vortex shedding through this approach is most likely achieved through significant alteration of the local mean velocity profiles with consequent reductions in the local absolute growth rates. The suppression of vortex shedding via insertion of a small control wire placed in the external flow close to the near wake (cf. Strykowski & Sreenivasan 1990) can be rationalized in a similar manner.

In a different approach, base bleed has been shown to be quite effective in reducing the strength of vorticity concentrations and the shedding frequency, even to the extent of suppressing shedding altogether (cf. Wood 1964, 1967; Bearman 1967; Hannemann, Lynn & Strykowski 1986; Hannemann & Oertel 1989; and Schumm *et al.* 1994). Since the region of absolute instability in the near wake exerts a dominant influence on the spatio-temporal dynamics of the wake, it seems clear that the use of blowing or suction from the base of the forebody can be used to alter local stability properties and, thereby, provide a mechanism for wake control or flow modification. In the earlier numerical experiment of Hannemann & Oertel (1989) on a symmetric wake, uniform blowing from the base was applied and a critical value was found for which vortex shedding was suppressed. From a global mode point of view, the velocity deficit in the near-wake profiles was reduced through base bleed rendering the flow less absolutely unstable and, eventually, decreasing the amplification of the global mode to negative values.

In the present study the effect of suction from the base region is investigated. In this case the velocity deficit near the base is expected to be deepened leaving the local flow more absolutely unstable. However, the application of suction should pull the near-wake saddle point of the time-averaged streamlines closer to the base, thereby decreasing the spatial extent of the region of absolute instability. Since the destabilization of a global mode requires that some integral measure of the absolute growth rate over the absolutely unstable region exceeds a critical value (like that proposed in (3.5)), there is an interesting competition occurring and the possible suppression of vortex shedding via suction is worth exploring.

A series of numerical simulations was performed with uniform suction across the

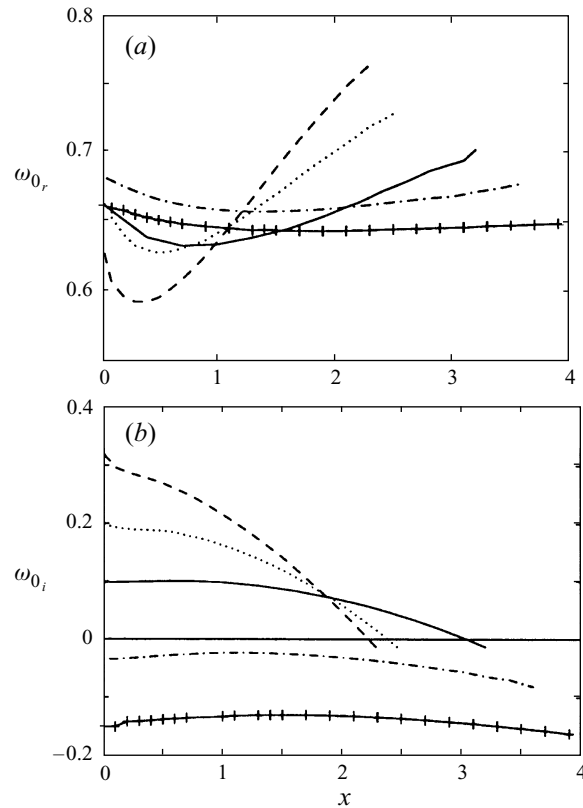


FIGURE 18. (a) The real absolute frequency and (b) the absolute growth rate of the asymmetric wake ($r = 0.2$) at $Re = 160$ without suction or blowing (—, $U_0 = 0$), subject to blowing (-+-+-+, $U_0 = -0.2$; ·····, $U_0 = -0.1$), and subject to suction (·····, $U_0 = 0.1$; - - - -, $U_0 = 0.2$).

base of the rectangular forebody to define the response of the wake to this technique for control. The first case considered was that of a sheared wake with $r = 0.2$ and $Re = 160$. As suction was increased gradually, the wake shedding frequency declined continuously until vortex shedding was abruptly suppressed at a suction velocity of $U_0 = 0.22$ and a completely steady wake flow appeared. The variation of the Strouhal number with suction velocity is shown in figure 17. The distribution of the absolute frequency was computed for cases with uniform suction or blowing. Results are shown in figure 18. One observes that the absolute growth rates increase with increasing suction in the very near-wake region, but that the streamwise extent of absolute instability is continuously shortened and the position of maximum absolute growth rate moves upstream, even to the trailing edge of the body. At the same time the minimum value of the frequency $\omega_{0,r}(x)$ decreases in magnitude consistent with figure 17, and the position of the minimum moves upstream.

Calculations of the location of the saddle point of $\omega_0(x)$ were not made for all the cases with suction because the location of the branch point of the dispersion relation, required for the evaluation of $\omega_0(x)$, became very difficult for mean velocity profiles near $x = 0$ where the shear layers in the wake became very thin. Nevertheless, it appears that this saddle point is very near, if not at, the trailing edge as the suction approaches its critical value for suppression of all global modes. Calculations of the saddle point x_s of $\omega_0(x)$ for low values of the suction velocity in a wake with

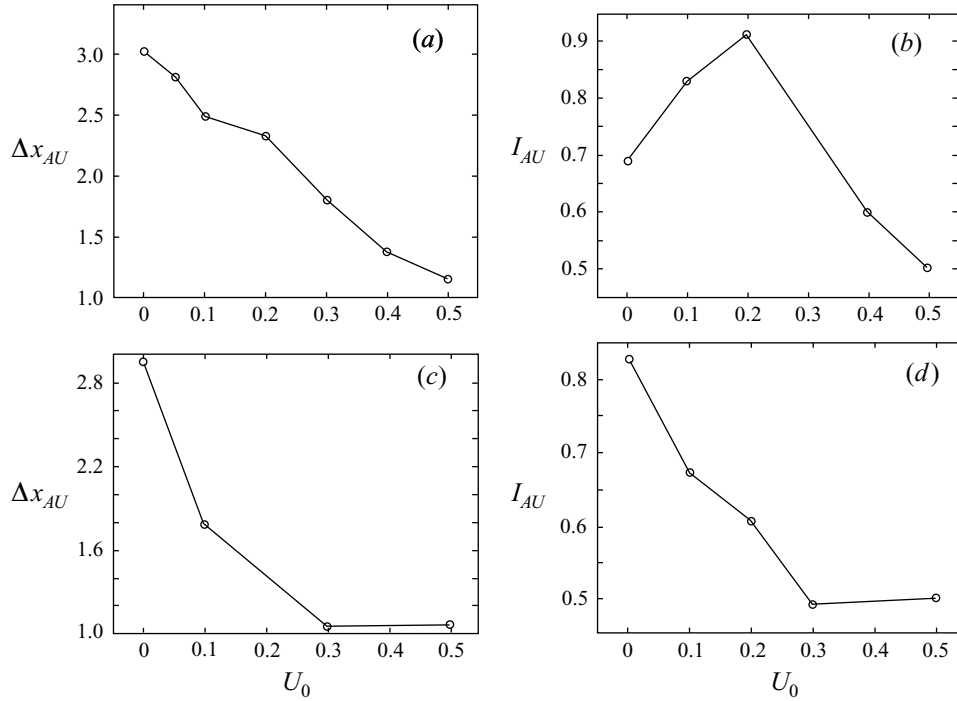


FIGURE 19. (a) The streamwise extent of the region of absolute instability and (b) the size of the absolute instability region as measured by the parameter I_{AU} for the asymmetric wake ($r = 0.2$) at $Re = 160$ and (c, d) likewise at $Re = 320$.

$r = 0.2$ and $Re = 160$ are given in table 4, together with the frequencies determined by the different selection criteria. The frequency prediction based on the saddle-point criterion without regard for the boundary condition imposed on the global mode by the presence of the body gives consistently better results.

The discrepancy between the predicted frequency and that observed in the full simulation increases slightly as the suction pulls the position of the saddle point toward the trailing edge. The flow becomes strongly non-parallel as the suction increases and the non-parallel corrections described in the Appendix, although not calculated, are expected to become increasingly important. The location of the downstream end of the absolutely unstable region, together with the value of the integral quantity in (3.5), is displayed in figure 19. The value of the integral I_{AU} becomes more sensitive to the value of $\omega_0(x)$ near the trailing edge as the suction is increased. At the same time, the evaluation of $\omega_0(x)$ becomes more difficult in this region. As a consequence, accuracy of the numerical values for I_{AU} is expected to decrease as the suction increases. For example, the initial rise in I_{AU} for $Re = 160$ as the suction increases toward the critical value is believed to be real, but the potential error bounds in the computed values also increase. Nevertheless, there is a clear decline in I_{AU} with increasing suction for $Re = 320$, and at higher suction velocities at $Re = 160$, and the distinct suppression of global dynamics beyond a critical suction velocity is firmly established.

Since base suction is found to be effective in damping all global modes, another sequence of simulations was performed for the purpose of evaluating the critical suction velocity for different flow conditions. The results are shown in figure 20.

U_0	x_{sr}	x_{si}	f	f_{sp}	f_k	f_p
0.00	0.81	0.132	0.1026	0.1035	0.1106	0.1038
0.05	0.64	0.088	0.1020	0.1021	0.1138	0.1025
0.10	0.47	0.079	0.0988	0.1000	0.1148	0.1038
0.15	0.38	0.111	0.0945	0.0979	0.1159	0.1050
0.20	0.33	0.148	0.0884	0.0956	0.1206	0.1019

TABLE 4. Saddle-point data and comparison of frequency selection criteria for asymmetric wakes with suction: $r = 0.2$, $Re = 160$.

In figure 20(a) the critical suction velocity is shown as a function of the Reynolds number at a fixed value of the velocity ratio $r = 0.2$. It is apparent that the value of $U_{0,crit}$ is approaching an asymptotic value as the Reynolds number increases. This is consistent with the experimental work of Leu & Ho (1993) where a critical suction velocity of approximately 0.5 is reported for a symmetric wake at $Re = 2000$. In their study the maximum absolute growth rate in the wake without suction was near 0.1, which is similar to the values we find here. However, the region of absolute instability extends to $x \simeq 4$ in their study while we find $x \simeq 3$. Figure 20(b) shows that the required suction velocity for suppressing global dynamics decreases, at fixed Reynolds number, as the asymmetry of the mean flow increases. The decrease is quite significant and is believed to be only slightly influenced by the fact that the critical Reynolds number for onset of global dynamics decreases slowly with increasing velocity ratio (cf. figure 12).

A very interesting result was observed when the suction equalled or exceeded the critical value for a sheared wake. With supercritical uniform suction from the base in a wake–shear layer, the steady, near-wake flow was observed to be directed (vectored) from the low-speed side toward the high-speed side. To quantify this effect, the saddle point of the near-wake streamline pattern was located in each computed realization for $r = 0.2$, $Re = 160$, and different applied suction velocities. When the suction is below critical and the global mode is active, the streamline pattern for the time-averaged flow was computed. When the suction is supercritical the entire flow is steady and a stationary streamline pattern persists. The angle between the x -axis and a line emanating from the origin at the centre of the base and extending through the computed saddle-point location was measured for each realization. The results are exhibited in figure 21. It is clear that a fairly abrupt symmetry-breaking is possible, but only when all global modes are suppressed. These ideas are pursued in a more comprehensive way in Hammond & Redekopp (1996) where the symmetry-breaking bifurcation is more abrupt at higher Reynolds numbers and deflection angles approaching 30° in each direction are shown to be possible by selective variations in the distribution of the suction velocity across the base. Before ending this section, however, we point out that the concepts associated with global mode dynamics are pivotal to the understanding of this vectored response and its initiation.

6. Conclusions

Numerical simulations, performed in conjunction with local instability calculations, have been performed for the purpose of validating the concept of a global mode in relation to the vortex shedding state. A global mode is a streamwise eigenmode characterized by a discrete frequency which synchronizes the dynamics over large

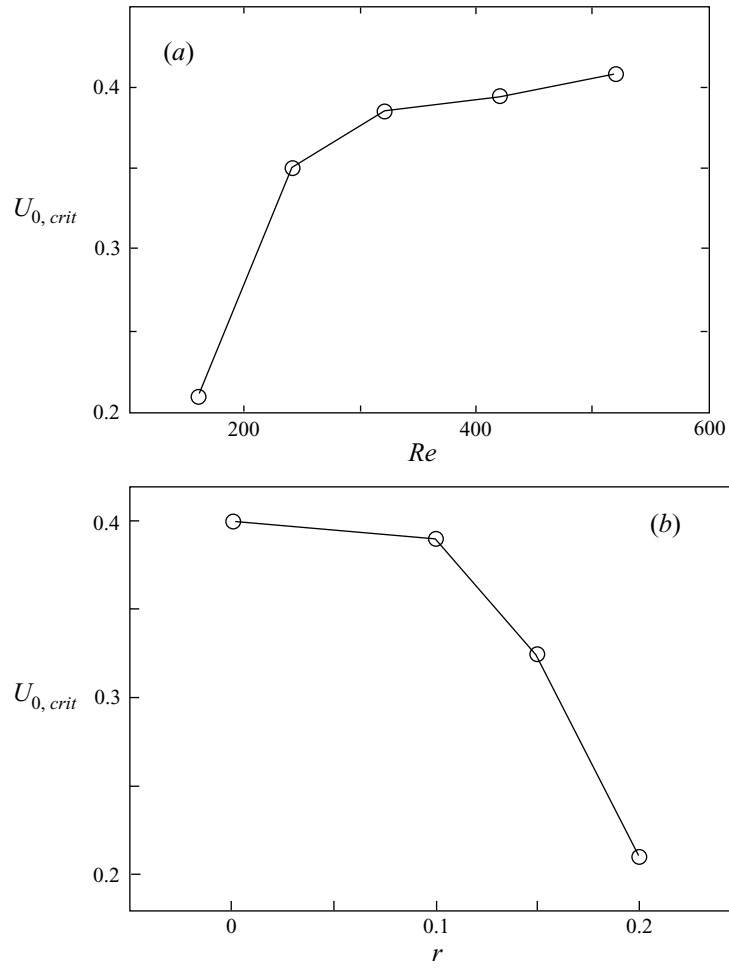


FIGURE 20. The critical suction velocity (a) versus Reynolds number at $r = 0.2$ and (b) versus velocity ratio at $Re = 160$.

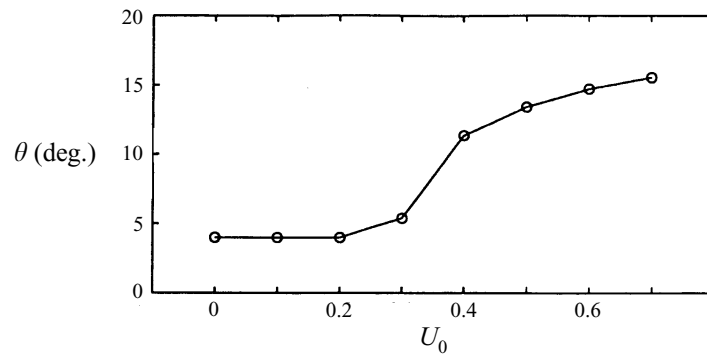


FIGURE 21. The angle of the vectored flow at $Re = 160$ and $r = 0.2$ and its dependence on the trailing-edge suction velocity U_0 .

streamwise extents. As described here for the wake of a flow over a rectangular forebody, the gravest global mode is destabilized by a supercritical Hopf bifurcation leading to spontaneous onset of vortex shedding. It has been demonstrated definitively that the normalized Landau coefficient for the local structure of the global Hopf bifurcation is a spatially uniform constant in the wake. This was also shown experimentally by Schumm *et al.* (1994). The intimate connection between the appearance of global dynamics via a global Hopf bifurcation and the existence of a pocket of local absolute instability has been clarified. The global mode shape for the symmetric wake has a streamwise structure with a single maximum in the near-wake region which exists downstream of the absolute instability region. This maximum corresponds quite closely to the region where concentrations of vorticity appear and the formation of the familiar vortex street occurs. The global mode of the asymmetric wake formed by the imposition of a persistent shear across the wake exhibits at least two local maxima in the streamwise variation of the amplitude of the global eigenmode. These streamwise modulations become more pronounced as the shear is increased.

The effects of suction, base-bleed, and shear have been studied and found to diminish the strength of the underlying global mode through their effect on the inherent potential of the absolute instability region in the near wake to induce globally coherent, discrete frequency oscillations. Suction has been shown to diminish the streamwise extent of the absolute instability region by pulling the downstream stagnation point in the near wake streamline pattern of the time-averaged flow toward the origin of the wake. Although the absolute growth rates in the near wake increase due to the increased backflow, the overall effect of suction is to reduce the potential of the absolute instability region to stimulate a global instability. When suction is increased beyond some critical value, which depends on the Reynolds number and the velocity ratio, the absolute instability region reduces sufficiently such that global instability criteria are no longer satisfied and the wake becomes steady and stable to, at least, small perturbations. Base bleed also has the effect of reducing the potential of the absolute instability region for global dynamics, primarily by decreasing the magnitude of the growth rates over the domain of absolute instability. The flow subject to supercritical base bleed also becomes steady and stable to perturbations. The influence of shear on the global stability of the flow has also been investigated. An imposed shear across the wake at fixed Reynolds number leads to a reduction in the magnitude of local absolute growth rates as well as a reduction in the streamwise extent of the absolute instability region. It is anticipated that at larger values of the shear, the global instability will be completely suppressed without the application of any control inputs such as base bleed or suction. As long as $r < 1$, the two ambient streams on opposite sides of the wake are co-flowing and the velocity deficit continuously relaxes in the downstream direction as the wake becomes dominated by shear layer type instabilities. Since shear layers do not exhibit global modes when the two streams are co-flowing, we anticipate the suppression of the global instability through the effect of shear alone to occur at some value of the velocity ratio less

rigorous proposal of a frequency selection criterion for a spatially developing flow, has been shown to provide surprisingly accurate frequency predictions. In the case of the symmetric wake at a supercriticality of $(Re - Re_{cr})/Re_{cr} = 0.33$, the saddle-point theory overpredicts the frequency by less than 1%. As the shear is increased and/or the suction velocity is increased, the saddle-point theory provides less accurate frequency predictions because at these conditions the mean flow deviates more severely from the weakly non-parallel, slightly supercritical conditions which were required for this theory. Nevertheless, the saddle-point theory does provide a surprisingly accurate prediction, even beyond the expected range of application.

This work was supported by AFOSR under Contract number F 49620-92-J-0377. Support for much of the computational effort was provided by the San Diego Super-computer Center. D. H. acknowledges partial support via a Rockwell International Graduate Fellowship. The authors acknowledge several fruitful discussions with P. Huerre.

Appendix

Monkewitz, Huerre & Chomaz (1993, hereinafter referred to as MHC), provided an analysis for the linear correction to the saddle-point frequency selection derived by Chomaz *et al.* (1991) arising from the spatially varying properties of the underlying waveguide. They presented a WKBJ analysis for weakly non-parallel shear flows at high Reynolds numbers. We describe here an application of their asymptotic theory using the spatially developing mean velocity profiles computed in the direct numerical simulation of the symmetric wake flow at $Re = 160$. Specifically, we compute the terms defined in equation (4.14) in MHC. With these terms to hand, the first correction to the global mode frequency based on the linearized saddle-point criterion can be found.

The MHC theory begins with the Rayleigh stability operator applied to the velocity profile $U(y; x_s)$ at the streamwise position x_s of the saddle point of the absolute frequency $\omega_0(x)$,

$$\mathcal{L}\phi_0 \equiv \left\{ (kU - \omega) \left(\frac{\partial^2}{\partial y^2} - k^2 \right) - kU'' \right\} \phi_0 = 0. \quad (\text{A1})$$

Primes are used here to denote differentiation with respect to the cross-stream coordinate y and (ω, k) form the frequency–wavenumber pair (ω_0, k_0) associated with the branch point values at this streamwise-position. Owing to the spatial non-uniformity of the flow, both the eigenfunction and the eigenvalues will change with streamwise position. The relevant corrections to the eigenfunction are represented by writing the streamwise gradient of $\phi_0(y; k, \omega, x)$ as

$$\frac{\partial \phi_0}{\partial x} = -\phi_{1k} \frac{\partial k}{\partial x} - \phi_{1\omega} \frac{\partial \omega}{\partial x} - \phi_{1x}. \quad (\text{A2})$$

The inhomogeneous equations for the indicated functions are as follows:

$$\mathcal{L}\phi_{1k} = \frac{\omega U'' - 2k(kU - \omega)}{kU - \omega} \phi_0; \quad (\text{A3})$$

$$\mathcal{L}\phi_{1\omega} = -\frac{kU''}{kU - \omega} \phi_0; \quad (\text{A4})$$

$$\mathcal{L}\phi_{1x} = k \left\{ \frac{kU''}{kU - \omega} \frac{\partial U}{\partial x} - \frac{\partial U''}{\partial x} \right\} \phi_0. \quad (\text{A5})$$

Analysis type	x_s	k_s	ω_s	$c_s = \omega_s/k_s$
Inviscid	$0.917 + 0.34i$	$1.209 - 0.747i$	$0.647 + 0.121i$	$0.343 + 0.311i$
Viscous	$0.737 + 0.074i$	$1.166 - 0.705i$	$0.632 + 0.1003i$	$0.359 + 0.302i$

TABLE 5. Comparison of saddle-point data from an inviscid and a viscous analysis.

Eigenfunction	k_0	ω_0	$c_0 = \omega_0/k_0$
ϕ_0	$1.209 - 0.747i$	$0.639 + 0.123i$	$0.337 + 0.310i$
ϕ_{1k}	$1.209 - 0.747i$	$0.663 + 0.130i$	$0.349 + 0.323i$
ϕ_{1x}	$1.209 - 0.747i$	$0.644 + 0.142i$	$0.333 + 0.323i$

TABLE 6. Modified eigenvalue data used for computation of respective eigenfunctions.

The solutions of (A3) and (A5) are needed, according to (4.14) in MHC, to evaluate the respective contributions to the first-order correction to the global mode frequency. The spatial non-uniformity of the mean flow is clearly evident in (A5). In practice, however, the calculation of the indicated derivatives of the mean velocity profile is a potential source of error. These derivatives were evaluated in the present work by using a forward difference formed by data at $(x_{sr} - \Delta x)$ and at x_{sr} , where $\Delta x = 0.1$ according to the nominal grid used in the simulation.

Since the MHC theory takes the Reynolds number to be sufficiently high so that the leading-order, local stability is based on inviscid theory, local stability calculations were made using the Rayleigh equation (A1). With the local dispersive properties known, the saddle point was located following equation (3.4) in the text and the saddle-point values (ω_s, k_s) were computed. These results are compared in table 5 with corresponding calculations based on a viscous, or Orr–Sommerfeld, analysis of the same mean profiles using the base Reynolds number $Re = 160$. The most striking difference is in the location of the saddle point.

Continuing with the inviscid theory and seeking to evaluate the functions ϕ_{1k} and ϕ_{1x} , another point of difficulty is encountered. The evaluation of these functions requires the computed values of the pair (ω, k) obtained from the branch-point calculation of the local dispersion relations at x_{sr} . Since these values are known only imprecisely, the solvability conditions for (A3) and (A5) are not satisfied exactly. As a consequence, application of a shooting algorithm with matching at some interior point is destined to fail. To circumvent this difficulty, we fixed the wavenumber at $k = k_s = k_0(x_s)$ and iterated the frequency (or phase speed c) until the solvability condition was satisfied. Using velocity data along the real line and the refined, or appropriately modified, eigenvalue pair (ω, k) , computation of the functions ϕ_{1k} and ϕ_{1x} was completed. Using velocity field data from the simulation with $r = 0$, $Re = 160$ and no suction/blowing (i.e. $U_0 = 0$), the functions shown in figure 22 were obtained. The iterated frequency–wavenumber pairs associated with these eigenfunction computations are listed in table 6. The entry for ϕ_0 has a different frequency and phase speed than that quoted in table 5 for the saddle point because the present results apply along the real line where the velocity profile data are known. Of course, as noted above, we have used the true k at the saddle point which is located 0.34 units above the real line as specified in table 5.

With the eigenfunctions ϕ_0 , ϕ_{1k} and ϕ_{1x} to hand, together with data for both the streamwise and transverse components of the mean velocity, the various quadratures

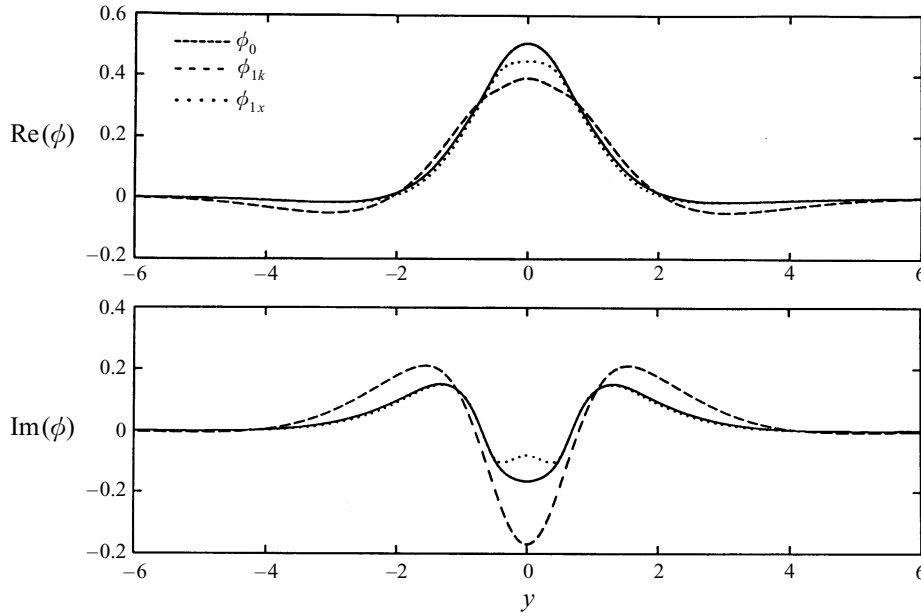


FIGURE 22. Eigenfunctions for $r = U_0 = 0, Re = 160$ used in computing the first correction to the global frequency.

appearing in equations (4.14 *a-d*) in MHC can be evaluated. Following the notation in MHC in exact sequence we obtain the following results:

$$\delta\omega^t = i \left\{ \frac{(0.0735 + 0.0856i) - (0.4721 - 0.3088i)}{0.1994 - 1.8503i} \right\} = 0.1902 - 0.2336i, \quad (\text{A6})$$

$$d_{kk}^t = \frac{2(0.0424 - 0.4791i) - (0.3226 + 0.5270i)}{0.1994 - 1.8503i} = 0.7798 - 0.2125i, \quad (\text{A7})$$

$$d_{kx}^t = \frac{(0.4721 - 0.3088i) + (0.07796 - 0.05627i) - (0.04428 + 0.1539i)}{0.1994 - 1.8503i} = 0.2462 + 0.2468i \quad (\text{A8})$$

$$d_{xx}^t = \frac{2(0.1025 + 0.1072i) - (0.00393 + 0.0776i)}{0.1994 - 1.8503i} = -0.0216 - 0.0298i. \quad (\text{A9})$$

Each of these expressions has the common denominator, denoted by $L_\omega^t(\phi_0^t)$ in MHC. These results allow calculation of the first correction to the global mode frequency resulting from the linear effects of flow non-uniformity. If the saddle-point location is isolated from boundaries, the complex global mode frequency is given by (6.2) in MHC. If the saddle point is close to a boundary, like the origin of the wake, the complex global mode frequency is given by (6.3) in MHC. The predicted and observed frequencies are summarized in table 7. The first correction, whether the saddle point is essentially isolated from the wake origin or close enough to be influenced by it, has a positive real part and a negative imaginary part. This correction, therefore, yields a Strouhal number that departs even further from the observed value. The correction to the imaginary part of the global frequency is also quite strong (i.e. the growth rate for the global mode). In fact, the correction is so strong for the doubly-infinite case where the saddle point is isolated that the global mode is predicted to be damped. Of

Source

- behind a flat plate with and without the influence of base bleed. *Internal Rep.* IB-221-86-A-26. DFVLR, Goettingen.
- HANNEMANN, K. & OERTEL, H. JR. 1989 Numerical simulation of the absolutely and convectively unstable wake. *J. Fluid Mech.* **199**, 55–88.
- HUERRE, P. & MONKEWITZ, P. A. 1990 Local and global instabilities in spatially developing flows. *Ann. Rev. Fluid Mech.* **22**, 473–537.
- KARNIADAKIS, G. E. & TRIANTAFYLLOU, G. S. 1989 Frequency selection and asymptotic states in laminar wakes. *J. Fluid Mech.* **199**, 441–469.
- KARNIADAKIS, G. E. & TRIANTAFYLLOU, G. S. 1992 Three-dimensional dynamics and transition to turbulence in the wake of bluff objects. *J. Fluid Mech.* **238**, 1–30.
- KOCH, W. 1985 Local instability characteristics and frequency determination of self-excited wake flows. *J. Sound Vib.* **99**, 53–83.
- KOVASZNAVY, L. S. G. 1949 Hot-wire investigation of the wake behind cylinders at low Reynolds numbers. *Proc. R. Soc. Lond. A* **198**, 174–190.
- LE DIZES, S., HUERRE, P., CHOMAZ, J.-M. & MONKEWITZ, P. A. 1996 Linear global modes in spatially-developing media. *Phil. Trans. R. Soc. Lond.* **354**, 169–212.
- LEONARD, B. P. 1979 A stable and accurate convective modelling procedure based on quadratic upstream interpolation. *Comp. Meth. Appl. Mech. Engng.* **19**, 59–98.
- LEU, T.-S. & HO, C.-M. 1993 Free shear layer control and its application to fan noise. *AIAA Paper* 93–3242.
- MATHIS, C., PROVANSAL, M. & BOYER, L. 1984 The Benard-von Karman instability: an experimental study near the threshold. *J. Phys. Lett.* **45**, 483–491.
- MATTINGLY, G. E. & CRIMINALE, W. O. 1972 The stability of an incompressible two-dimensional wake. *J. Fluid Mech.* **51**, 233–272.
- MONKEWITZ, P. A. 1988 The absolute and convective nature of instability in two-dimensional wakes at low Reynolds numbers. *Phys. Fluids* **31**, 999–1005.
- MONKEWITZ, P. A. 1989 Feedback control of global oscillations in fluid systems. *AIAA Paper* 89–0991.
- MONKEWITZ, P. A. 1993 Wake control. In *Bluff-Body Wakes, Dynamics and Instabilities* (ed. H. Eckelmann, J. M. R. Graham, P. Huerre & P. A. Monkewitz), pp. 227–290. Springer.
- MONKEWITZ, P. A., HUERRE, P. & CHOMAZ, J.-M. 1993 Global linear stability analysis of weakly non-parallel shear flows. *J. Fluid Mech.* **251**, 1–20 (referred to in the Appendix as MHC).
- OERTEL, H. JR. 1990 Wakes behind blunt bodies. *Ann. Rev. Fluid Mech.* **22**, 539–564.
- PARK, D. S. & REDEKOPP, L. G. 1992 A model for pattern selection in wake flows. *Phys. Fluids A* **4**, 1697–1706.
- PIERREHUMBERT, R. T. 1984 Local and global baroclinic instability of zonally varying flow. *J. Atmos. Sci.* **41**, 2141–2162.
- PROVANSAL, M., MATHIS, C. & BOYER, L. 1987 Benard-von Karman instability: transient and forced regimes. *J. Fluid Mech.* **182**, 1–22.
- ROSHKO, A. 1954 On the drag and shedding frequency of bluff cylinders. *NACA TN* 3169.
- SCHUMM, M., BERGER, E. & MONKEWITZ, P. A. 1994 Self-excited oscillations in the wake of two-dimensional bluff bodies and their control. *J. Fluid Mech.* **271**, 17–53.
- SREENIVASAN, K. R., STRYKOWSKI, P. J. & OLINGER, D. J. 1986 Hopf bifurcation, Landau equation, and vortex shedding behind circular cylinders. *Proc. Forum on Unsteady Flow Separation* (ed. K. H. Ghia). ASME FED vol. 52.
- STRYKOWSKI, P. J. & SREENIVASAN, K. R. 1990 On the formation and suppression of vortex shedding at low Reynolds number. *J. Fluid Mech.* **218**, 71–107.
- TRIANAFYLLOU, G. S., KUPFER, K. & BERS, A. 1987 Absolute instabilities and self-sustained oscillations in the wakes of circular cylinders. *Phys. Rev. Lett.* **59**, 1914–1917.
- TRIANAFYLLOU, G. S., TRIANTAFYLLOU, M. S. & CHRYSOSTOMIDIS, C. 1986 On the formation of vortex streets behind stationary cylinders. *J. Fluid Mech.* **170**, 461–477.
- TRITTON, D. J. 1959 Experiments on the flow past a circular cylinder at low Reynolds numbers. *J. Fluid Mech.* **6**, 547–567.
- WALLACE, D. A. & REDEKOPP, L. G. 1991 Linear instability characteristics of wake-shear layers. *Phys. Fluids A* **4**, 189–191.
- WILLIAMSON, C. H. K. 1988 Defining a universal and continuous Strouhal-Reynolds number relationship for the laminar vortex shedding of a circular cylinder. *Phys. Fluids* **31**, 2742–2744.

- WILLIAMSON, C. H. K. 1989 Oblique and parallel modes of vortex shedding in the wake of a circular cylinder at low Reynolds numbers. *J. Fluid Mech.* **206**, 579–627.
- WOOD, C. J. 1964 The effect of base bleed on a periodic wake. *J. R. Aero. Soc.* **68**, 477–482.
- WOOD, C. J. 1967 Visualization of an incompressible wake with base bleed. *J. Fluid Mech.* **29**, 259–272.
- ZEBIB, A. 1987 Stability of viscous flow past a circular cylinder. *J. Engng Maths* **21**, 155–165.